

Table 1. Liposomes Used in the Study

liposome composition	lipid mole ratio	mean diameter (intensity weighted), nm	PDI
EPC/DSPE-PEG-2000/DiI	94.75/5/0.25	174	0.107
EPC/DSPE-PEG-2000/DiR	94.75/5/0.25	263	0.197
EPC/DiI	99.75/0.25	197	0.063
EPC/DSPE-PEG-2000/DiI/DiR	94.5/5/0.25/0.25	255	0.233
EPC/DiI/DiR	99.5/0.25/0.25	300	0.225
LipoDox HSPC/Chol/DSPE-PEG-2000	56.6/38.2/5.2	88	0.047
HSPC/Chol/DSPE-PEG/DiI	56.35/38.2/5.2/0.25	135	0.19

pressure, hence termed “foot and hand syndrome” (also called palmoplantar erythrodysesthesia, or PPE).^{2,3} In addition to PPE, patients develop a diffuse follicular rash, eruptions, and hyperpigmentation.⁴ This unusual toxicity is caused by accumulation of liposomes in the dermis and release of the anticancer drug locally.³ Some early classical studies of accumulation of PEGylated liposomes in leaky tumor vasculature showed a significant accumulation in the healthy skin surrounding tumors.^{5–7} Several other studies have also indicated efficient skin accumulation of blood-stable phosphatidylcholine/cholesterol liposomes,^{8,9} with up to 5% of injected dose per gram of skin tissue.⁷ Besides liposomes, other PEGylated nanoparticle types can accumulate in the skin, primarily in macrophages and dendritic cells.^{2,10,11}

Previously, we used fiber optical near-infrared spectroscopy (FONIRS) to monitor levels of near-infrared dye-labeled liposomes and biologics in BALB/c and nude mouse skin after systemic injection.¹² We found that PEGylated egg phosphatidylcholine (EPC) liposomes result in a much higher near-infrared fluorescence in the skin than non-PEGylated vesicles. In addition, the fluorescence signal was retained for up to 7 days. While the pharmacokinetics of skin accumulation of liposomes as a function of composition have been documented,^{9,8,9} the dynamics at the microscopical level is poorly understood. Here, we used intravital microscopy to dissect fine details of skin accumulation of PEGylated and non-PEGylated liposomes. We found that aggregation in circulation contributes toward fast accumulation of non-PEGylated liposomes in the skin vasculature. PEGylated liposomes did not undergo aggregation but surprisingly quickly lodged in the endothelium and then within few hours extravasated the capillaries and became internalized by phagocytic cells in the skin. Skin accumulation was not mediated by complement and was not due to transport by circulating leukocytes and platelets. This study contributes to our understanding of skin deposition of nanocarriers in order to improve the safety of systemically injected drug delivery systems.

RESULTS

Non-PEGylated Liposomes Show *in Vivo* Aggregation and Rapid Skin Deposition. We prepared large unilamellar non-PEGylated liposomes composed of EPC. The liposomes were labeled with 0.25 mol % of DiI and/or DiR in order to enable tracking with intravital microscopy and near-infrared imaging, respectively. DiI and DiR are similar lipophilic cyanine dyes, with DiI having a spectrum close to that of Cy3 (visible fluorescence), whereas DiR has a spectrum similar to that of Cy7 (near-infrared fluorescence). The lipophilic cyanine dyes are extremely photostable, are tightly integrated in bilayers, and are not readily exchangeable *in vitro* and *in vivo*.^{13–15} As shown in Table 1, non-PEGylated DiI/DiR labeled EPC-based liposomes were approximately 300 nm in size. Following

systemic injection, the liposomes were cleared from the blood with a half-life of 1.3 h (Figure 1A), consistent with a short half-life previously observed for non-PEGylated liposomes.¹⁶ Fiber optical NIR spectroscopy (FONIRS) of mouse skin showed a spike in fluorescence at 5 min postinjection, which decreased by 70% at 5 h but stayed above the baseline for 7 days post injection (Figure 1B).

To study the dynamics of localization of liposomes, we performed intravital confocal microscopy at different time points postinjection. Intravital microscopy is an emerging tool to study real-time behavior of nanocarriers and biomolecules in intact tissues at cellular and subcellular resolution.^{17,18} Mice were preinjected with non-PEGylated EPC/DiI liposomes and immediately prior to the imaging were injected with 2 MDa FITC-dextran (a blood vessel marker) and Hoechst (nuclear marker) as described in Figure 1C. The imaging was performed on the visceral side of the abdominal skin flap (Figure 1C). At 4.5 h postinjection, the liposomes were bound to blood vessel lumen, as evidenced by colocalization with FITC-dextran (Figure 1D (upper left) and video 1). At 24 h postinjection, the localization of liposomes was both intravascular and extravascular (Figure 1D, upper right and video 2). At 48 h postinjection, we observed fluorescence both in blood vessels and in cells outside the blood vessels (Figure 1D, lower left). Control noninjected mice did not show visible fluorescence in the red channel (Figure 1D, lower right). These data suggest that EPC/DiI liposomes bind to blood capillaries and subsequently extravasate. Since most of the liposomes cleared within a few hours (Figure 1A, arrow), we decided to investigate the early dynamics by time-lapse videomicroscopy immediately after injection of EPC/DiI liposomes (Figure 1C). The movie was recorded for 2 h 15 min. As shown in selective frames in Figure 1E and in video 3, large fluorescent particles sized over 1 μm in diameter continuously circulated in the blood and started to accumulate in blood vessel lumens around 1 h postinjection. These particles were unlabeled by Hoechst staining, confirming that they are not blood leukocytes. Aggregation of non-PEGylated liposomes in serum has been described previously.^{16,19} Incubation of liposomes in fresh mouse serum *in vitro* resulted in formation of large fluorescent aggregates (Figure 1F). To test for liposomal aggregation *in vivo*, we isolated blood from mice 10 min postinjection and separated plasma from blood cells. As shown in Figure S1A, there were many large (over 1 μm) aggregates in plasma but very few in the washed blood cell fraction. There was no evidence of fluorescently labeled platelets or leukocytes in blood. These data suggest that EPC/DiI liposomes undergo aggregation after systemic injection and the observed aggregates lodge in the capillaries.

PEGylated Liposomes Show Rapid Deposition in Skin Capillaries, Efficient Extravasation, and Retention. Next, we prepared PEGylated liposomes made from EPC and

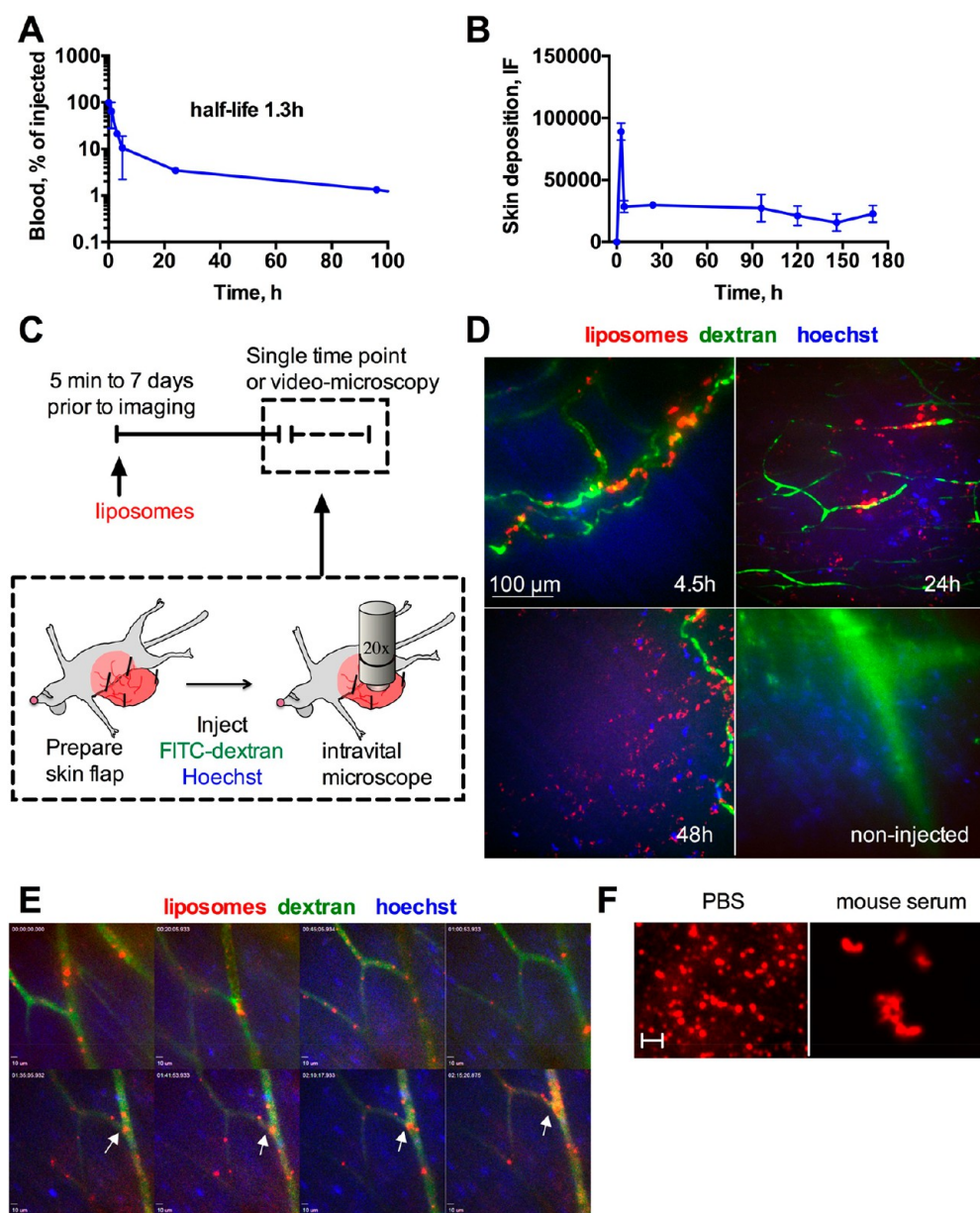


Figure 1. Dynamics of accumulation of non-PEGylated liposomes in mouse skin: Mice were injected with EPC/DiI or EPC/DiR liposomes. (A) Blood clearance profile (monoexponential curve fit) of liposomes after systemic injection ($n = 2$). (B) Skin NIR fluorescence monitored with fluorescence spectroscopy (FONIRS). The contribution of blood pool was subtracted as described in the **Methods**. Note that DiR fluorescence persisted after the liposomes had cleared from the blood (arrow). $n = 3$. (C) Schematic of intravital imaging experiments. Hoechst and FITC-dextran were used for intravital nuclear staining and blood vessels contrast, respectively. The imaging setup shows the abdominal skin flap and the objective facing the subdermis. (D) intravital images (maximum projections of z-stacks) of skin at different times postinjection. At 24 and 48 h, there was fluorescence accumulation outside blood vessels. Corresponding 3-D movies are provided as [video 1](#) and [video 2](#). Size bar is the same for all images. (E) Selected frames of a video taken as soon as 5 min postinjection for duration of 2 h 15 min ([video 3](#)). Arrows point to large fluorescent particles that start to build up in capillaries at approximately 1.5 h postinjection. All experiments were repeated at least two times. (F) Liposomes show aggregation in mouse serum *in vitro* and in blood *in vivo* ([Figure S1](#)), suggesting that circulating particles observed in (E) are likely liposomal aggregates. Scale bar = 2 μm .

distearoylphosphatidylethanolamine PEG-2000 (DSPE-PEG-2000). The liposomes were labeled with DiI for live microscopy and/or with DiR for combined microscopy and near-infrared imaging. According to [Table 1](#), the liposomes were sized around 255 nm. Following systemic injection, the liposomes were slowly eliminated from the blood with a monoexponential half-life of ~ 22 h ([Figure 2A](#)). FONIRS measurements of DiR fluorescence in the skin showed a steady increase up to 24 h postinjection and a slow decrease thereafter ([Figure 2B](#)). At 7

days, the level of fluorescence was about 3-fold higher than for non-PEGylated liposomes. Intravital microscopy at different time points showed that as soon as 5 min postinjection there was already intravascular deposition ([Figure 2C](#), upper left). Thirty minutes postinjection, some of the fluorescence appeared to be localized in the endothelium lining of the blood vessels rather than in the lumen ([Figure 2C](#), upper right, and [video 4](#)). At 3 h postinjection, there was a significant accumulation of liposomal fluorescence in cells outside blood

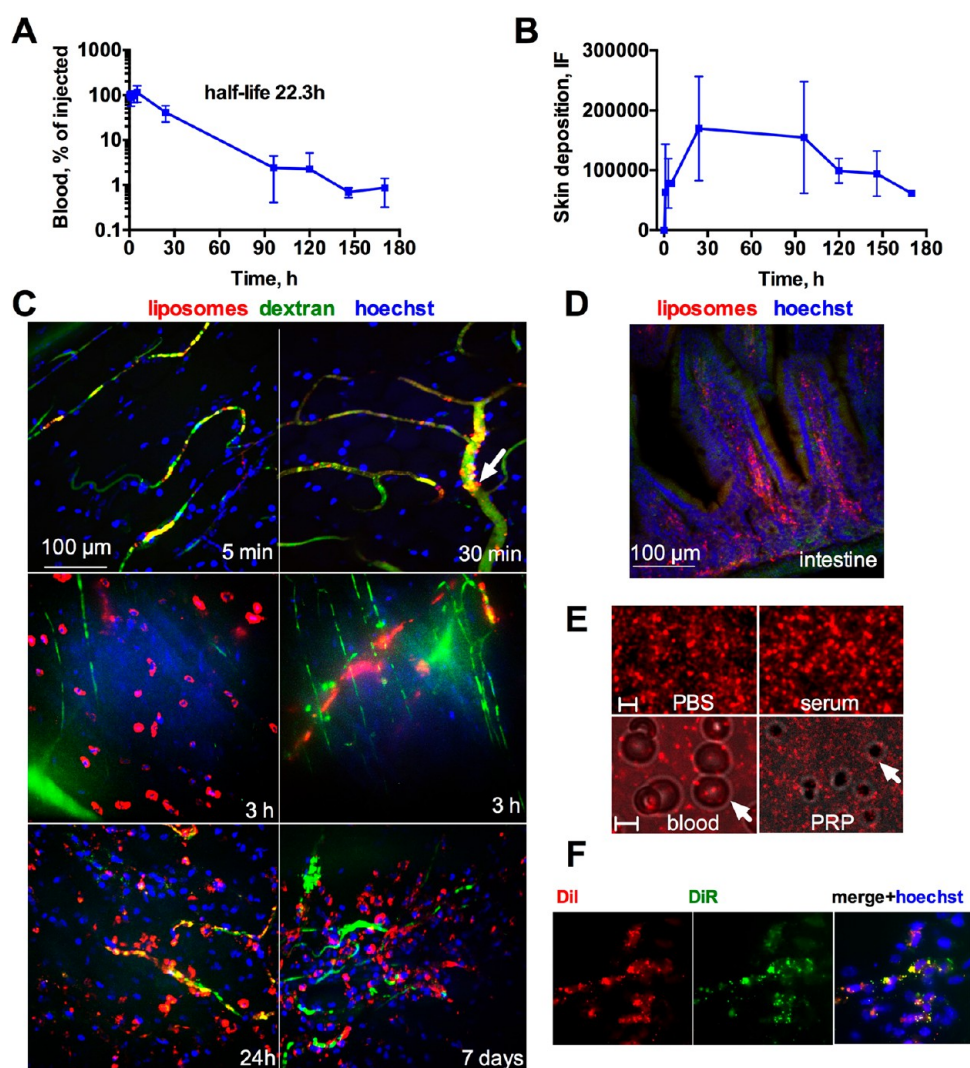


Figure 2. Dynamics of accumulation of PEGylated liposomes in mouse skin. Mice were injected with EPC/DSPE-PEG-2000/DiI or EPC/DSPE-PEG-2000/DiR liposomes. (A) Blood clearance profile (monoexponential curve fit) of liposomes after systemic injection shows long half-life of 22 h ($n = 3$). (B) Skin fluorescence with FONIRS shows slower buildup than non-PEGylated liposomes and prolonged retention after the liposomes had cleared from the blood (arrow); $n = 3$. (C) Intravital images (maximum projections of z-stacks) of skin at different times postinjection. Note the mostly intravascular deposition at early time points, some endothelial deposits (30 min, arrow) and massive extravasation of liposomes at later time points (3 h, 24 h and 7 days). Animated 3-D images are provided as [video 4](#) and [video 5](#). Size bar is the same for all images. (D) Histological section of small intestine (other organs are in [Figure S2](#)) at 7 days postinjection shows accumulation in microvilli. (E) Aggregation of liposomes was studied under fluorescent microscope. PEGylated liposomes do not show aggregates in serum *in vitro* and *in vivo* (whole blood and platelet rich plasma (PRP)). There was minimal binding to blood cells and platelets ([Figure S3](#)). Arrows point to RBC and platelet. Scale bar = 2 μm for the upper panel, 5 μm for the lower panel. (F) DiI and DiR fluorescence was mostly colocalized in the skin 24 h postinjection of DiI/DiR-labeled PEGylated liposomes, suggesting that liposomes arrived intact to the skin.

vessels ([Figure 2C](#), middle left), in addition to intravascular deposits ([Figure 2C](#), center right). Between 24 h and 7 days postinjection, we observed massive accumulation of liposomes in cells outside the blood vessels ([Figure 2C](#), lower panel, and [video 5](#)), but some fluorescence was still confined to the vasculature. As shown in histological sections taken 7 days postinjection ([Figure 2D](#) and [Figure S2A](#)), in addition to the skin there was a significant deposition in the small intestine, liver, and spleen, but not the muscle, kidney, brain, and lung. Notably, in the small intestine the fluorescence was localized in the capillary-rich center of microvilli ([Figure 2D](#) and [Figure S2A](#)). Intestinal capillaries have a discontinuous diaphragm,^{20,21} which could explain the significant deposition of liposomes. Post-mortem NIR fluorescence of organs of mice injected with DiR PEGylated liposomes was consistent with the histological

observations ([Figure S2B](#)). Interestingly, the gallbladder did not contain any DiR fluorescence ([Figure S2C](#)), suggesting that secretion via biliary tract is not responsible for the high signal in the intestine.

Intrigued by the fast (within 5 min postinjection) deposition of fluorescence in the skin capillaries ([Figure 2C](#), upper panel), we questioned if the liposomes were still intact after the injection. Images of liposomes in PBS or mouse serum *in vitro* and images of plasma and blood cells recovered *in vivo* 15 min postinjection showed the absence of aggregates and no visible uptake by blood cells ([Figure 2E](#) and [Figure S3](#)). Moreover, in contrast to a previous report on the uptake of PEGylated liposomes by platelets after injection into mice,²² we did not observe fluorescent platelets in platelet-rich plasma ([Figure S3](#)). In order to address the concern that the fluorescent label

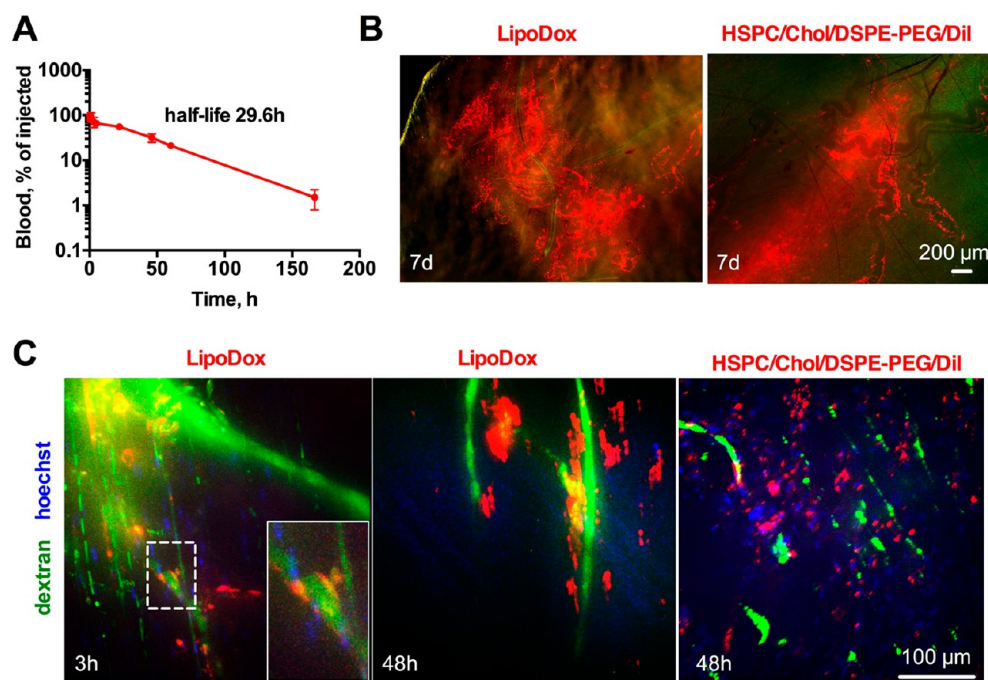


Figure 3. LipoDox (PEGylated liposomal doxorubicin) and PEGylated HSPC/Chol liposomes shows dynamics of deposition similar to PEGylated EPC liposomes. LipoDox was injected at 2 mg/kg (doxorubicin) into Balb/C mice. (A) Circulation half-life (monoexponential curve fit) of LipoDox in plasma ($n = 2$). (B) Low magnification *ex vivo* images of skin of mice injected with LipoDox or HSPC/Chol/DSPE-PEG-2000/DiI (7 days postinjection) show massive deposition of fluorescence. Some fluorescence follows the outside contour of blood vessels and the distribution of the liposomes is heterogeneous. (C) Intravital microscopy of skin of mice injected with LipoDox or HSPC/Chol/DSPE-PEG-2000/DiI shows localization in blood vessels and extravasation. The doxorubicin fluorescence, which was dimmer than DiI due to mismatch of Dox fluorescence with the optical setup of the intravital microscope, was enhanced in both images to the same extent. Animated 3-D images are provided as [video 6](#) and [video 7](#).

dissociated from liposomes soon after the injection, non-PEGylated or PEGylated EPC liposomes were incubated in mouse serum for 1 h and analyzed for the presence of the dye in serum supernatant (after pelleting the liposomes by ultracentrifugation). There was a minimal transfer of the dye to serum as over 94% of the fluorescence was pelleted by centrifugation (Figure S4), excluding the possibility that the dye is lost by transfer to serum. Moreover, DiR/DiI labeled PEGylated EPC liposomes showed colocalization of both dyes in histological sections of the skin at 24 h postinjection (Figure 2F), suggesting that liposomes did not fall apart after the injection.

Despite the evidence that PEGylated EPC liposomes do not aggregate and do not transfer the dye to serum, we performed further studies using liposomes of different lipid composition. Liposomes composed of saturated lipids with high transition temperature (e.g., distearoyl PC (DSPC), hydrogenated soy PC (HSPC)) and cholesterol exhibit high serum stability.^{23–25} We used liposomal doxorubicin (LipoDox) sized ~ 90 nm and composed of HSPC/Chol/DSPE-PEG-2000 and also prepared ~ 130 nm liposomes of the same composition but labeled with DiI (Table 1). As shown in Figure 3A, LipoDox showed long blood circulation time with a monoexponential decay of 29 h half-life (Figure 3A). Low-magnification *ex vivo* images of freshly excised skin showed widespread accumulation of the doxorubicin fluorescence 7 days postinjection (Figure 3B, left). Some of the fluorescence was perivascular, and the distribution was heterogeneous. Empty liposomes showed a similar pattern of DiI accumulation (Figure 3B, right). Intravital imaging of mice injected with LipoDox at 3 h postinjection showed deposition of doxorubicin both in the endothelium and outside

the vasculature (Figure 3C and video 6), whereas imaging at 48 h postinjection showed mainly extravascular deposition (Figure 3C and video 7). Imaging of empty PEGylated liposomes at 48 h showed extensive extravascular deposition of fluorescence, similar to that of LipoDox and PEGylated EPC liposomes. Incubation of empty PEGylated liposomes in mouse serum did not result in a significant dye transfer (Figure S4). These data confirm that the observed dynamics of skin deposition is typical for many liposomal types regardless of composition and labeling type (doxorubicin versus DiI).

Accumulation of PEGylated Liposomes in the Skin Is Independent of PEGylation Level, Complement, Leukocytes, and Platelets. Due to our observation that skin deposition of liposomes involves initial interaction with blood vessels, subsequent extravasation and uptake by extravascular cells, we asked whether PEG-2000 at 5 mol % is inadequate to prevent interactions with the skin. Previously, it has been shown that “backfilling” the gaps in the PEG layer of nanoparticles with shorter PEG chains can minimize non-specific interactions with proteins.²⁶ Therefore, we prepared EPC-based liposomes in which DSPE-PEG-2000 was combined with DSPE-PEG-700 or DSPE-PEG-350 to backfill the spaces between the longer PEG chains. According to *ex vivo* NIR scans of excised skin 7 days postinjection, inclusion of shorter PEGs into the EPC/DSPE-PEG-2000 liposomes was ineffective at reducing the level of accumulation in the skin (Figure 4).

Despite the fact that we did not observe uptake of liposomes by leukocytes in blood (Figure S3), we nevertheless performed additional studies to exclude the possibility that circulating leukocytes take up liposomes and “drive” them across the endothelium. Thus, several studies have demonstrated uptake

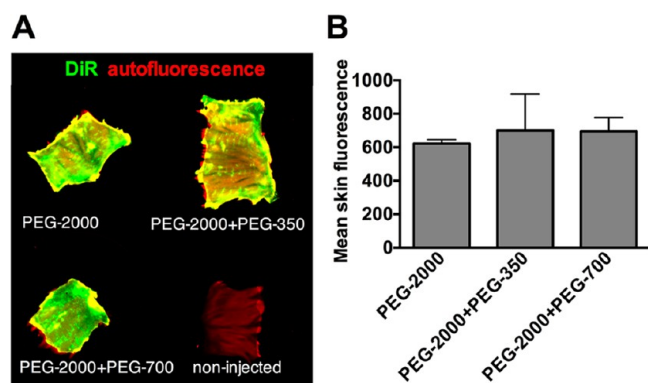


Figure 4. Backfilling with shorter PEGs does not affect the level of skin deposition. EPC liposomes were formulated with EPC/DSPE-PEG-2000 and either DSPE-PEG-350 or DSPE-PEG-700 as described in the [Methods](#). (A) Whole skin pieces (approximately 4 cm × 3 cm) were collected post-mortem and scanned with LiCOR Odyssey at 800 nm (DiR) and 700 nm (skin autofluorescence). Representative images are shown. All groups showed accumulation of DiR, regardless of the PEG size. (B) Mean fluorescence intensity quantification showed no difference between experimental groups (p value 0.22; $n = 3$, two tailed unpaired t test).

of nanoparticles by circulating leukocytes,^{27,28} and these cells are known for their ability to extravasate into inflamed tissues.²⁹ Uptake of nanoparticles and liposomes by leukocytes predominantly depends on complement opsonization (C3b and/or iC3b).^{27,28,30} Injection of either EPC/DSPE-PEG-2000 liposomes or LipoDox into C3 deficient mice did not decrease the level of accumulation in the skin compared with wild type mice ([Figure S5](#)). Neutrophils and monocytes in mice can be depleted by pretreatment with anti-Ly6C antibody.³¹ However, pretreatment of mice with anti-Ly6C (see the [Methods](#)) did not block the extravasation of liposomes and uptake by extravascular cells ([Figure 5A](#)) and only marginally decreased the skin fluorescence ([Figure 5B](#)). The minor decrease could be due to the fact that Ly6C is expressed on monocytes, which are progenitors of skin dendritic cells.³² Immunostaining showed minimal colocalization of DiR fluorescence with the pan-leukocyte marker CD45³³ ([Figure 5C,D](#)). There was also no colocalization of DiI with CD41⁺ platelets in the tissue ([Figure 5C,D](#)). At the same time, some of the liposomes were still localized in CD31-positive blood vessels ([Figure 5C](#)). Collectively, our data suggest that leukocytes and platelets do not take up PEGylated liposomes and are not responsible for the binding to and transport across the endothelium. On the other hand, liposomes significantly colocalized with F4/80⁺ cells ([Figure 5D,E](#)), which are likely skin dendritic cells.³⁴

DISCUSSION

Previous studies^{8,9} showed efficient accumulation of liposomes in the skin, but this is the first study of dynamics of liposomal accumulation at the microscopical level. We demonstrated that systemically injected PEGylated and non-PEGylated liposomes bind to the endothelium of skin capillaries and subsequently accumulate in extravascular cells in the dermis and subdermis. The dynamics of skin accumulation is different for the two types of liposomes. Non-PEGylated liposomes showed immediate aggregation *in vivo* and subsequent lodging of circulating aggregates in the vasculature. The reason for the aggregation may involve binding of liposomes to plasma

components such as lipoproteins and apolipoproteins, causing phase separation and fusion.²⁴ On the other hand, PEGylated liposomes showed minimal aggregation but paradoxically more efficient and prolonged accumulation. The dynamics of extravasation and extravascular deposition was similar for EPC-based and HSPC/cholesterol-based PEGylated liposomes, despite the fact that cholesterol-rich liposomes are more stable than cholesterol-poor liposomes, and have shown less phospholipid exchange with lipoproteins (or phospholipid transfer to lipoproteins).^{23,24} Unexpectedly, soon after the injection many cells outside blood vessels internalize liposomes. Dendritic cells, Langerhans cells, or other subtypes of skin phagocytes are positive for F4/80,³⁵ but further molecular profiling would be necessary to elucidate the exact cell type. It is not clear at the moment why PEGylated long-circulating “stealth” liposomes (half-life 22 h for EPC-based liposomes and 29 h for LipoDox) show such a fast uptake by skin phagocytes. One explanation could be that PEG only decreases uptake by macrophages, but never completely blocks it. Indeed, *in vivo* uptake of long-circulating nanoparticles by various subsets of macrophages has been reported before.^{36,37} Another explanation could be that after extravasation the liposomes lose their PEG coating and become more susceptible to the uptake by phagocytes.

While several different mechanisms can be proposed to explain the binding of liposomes to the vascular endothelium and subsequent movement outside the capillaries, we can eliminate some possibilities. Our data suggest that circulating neutrophils and platelets do not play a key role in endothelial cell binding and extravasation of PEGylated liposomes. In addition, we showed that complement, which is the main opsonin that mediates uptake of liposomes and nanoparticles by neutrophils,^{27,28,30} does not play a significant role either. It is unlikely that liposomes penetrate the skin via leaky vasculature, akin to the enhanced permeability and retention (EPR) effect in solid tumors.³⁸ In fact, normal capillaries in the skin are not porous³⁹ and are not permeable to molecules larger than 70 kDa.⁴⁰ Liposomal doxorubicin does not show permeability in capillary systems with tight junctions, such as in the heart, hence, the reduced cardiac toxicity.⁴¹ One possible mechanism, which is consistent with our data, is the uptake of liposomes or liposomal aggregates by endothelial cells and subsequent transcytosis. Binding of apolipoproteins to non-PEGylated as well as PEGylated liposomes and nanoparticles is a well-described phenomenon,^{24,42} and apolipoproteins may mediate vesicle recognition by endothelial cells through scavenger receptors or lipoprotein receptors. For instance, endothelial scavenger receptor LOX-1 is the receptor for oxidized lipoproteins⁴³ and is known to reside in cholesterol-rich lipid rafts.⁴⁴ Previous studies have demonstrated the role of caveolae-mediated endocytosis in transport of lipoproteins across the endothelium.⁴⁵ Nanoparticles can be taken up *via* a caveolae-dependent mechanism, albeit with size limitations.⁴⁵ In addition to caveolae, transport across the endothelial barrier might involve the exosomal pathway.^{46,47} One possible clue to understanding mechanisms of skin accumulation is the heterogeneity of liposomal distribution. In patients, foot and hand syndrome is restricted to areas of pressure and mucous membranes. While focal distribution of liposomes in patients is not known (the symptoms only point to the areas where the active drug is released), in mice we also observed heterogeneity of distribution (e.g., [Figure 3B](#), [4A](#), [5B](#)). It is possible that transient deformation and inflammatory stimuli contribute to

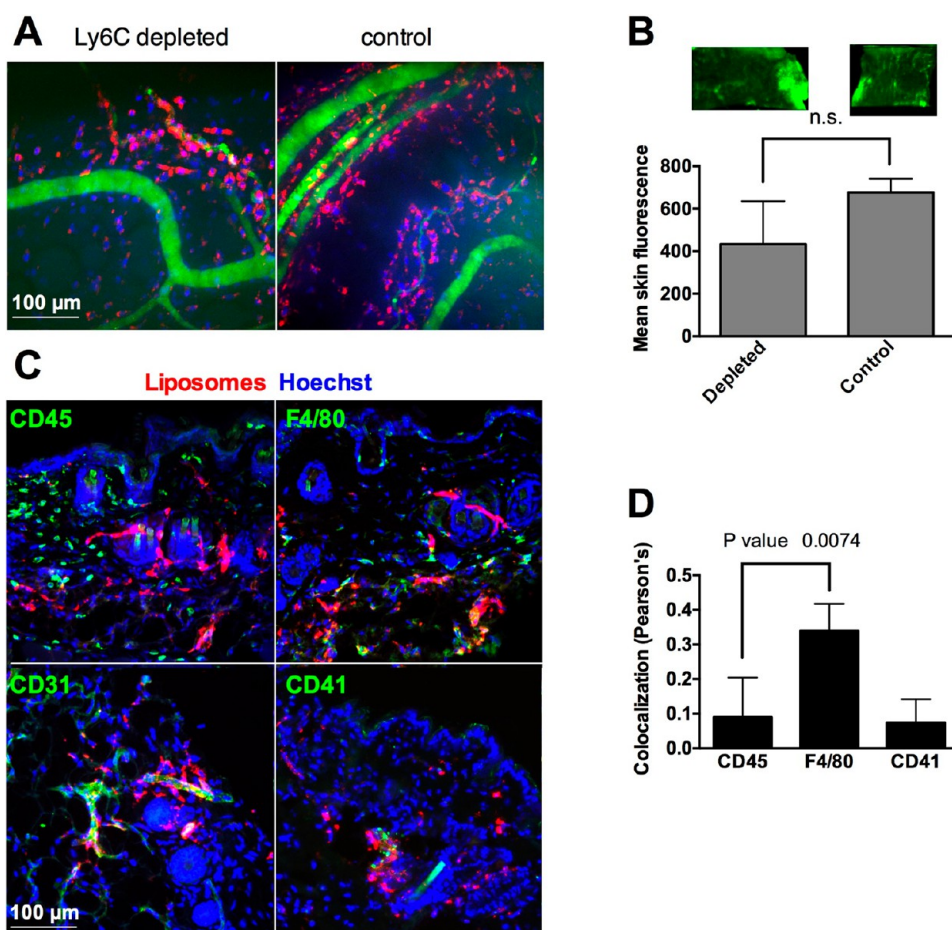


Figure 5. Accumulation of PEGylated liposomes is independent of leukocytes and platelets. (A) Neutrophils were depleted with Ly6C-specific antibody as described in the [Methods](#). Intravital imaging of skin 7 days postinjection shows similar extravasation and deposition of liposomes in depleted and control mice. (B) Representative scan of skin and mean fluorescence quantification show nonsignificant decrease in the accumulation in the depleted mice (p value 0.06, two-tailed unpaired t test, $n = 3$). (C) Immunostaining of skin histological sections 7 days postinjection shows minimal colocalization of liposomes with CD45+ leukocytes, CD41+ platelets, but colocalization with F4/80+ phagocytes (likely dendritic cells). Note that leukocytes are homogeneously distributed, F4/80+ cells are segregated in dermal and subdermal layers, and platelets are mostly limited to large blood vessels. Some liposomes were still located in the blood vessels (CD31+). (D) Colocalization analysis of the three stains in (C) with the liposomes (Pearson's correlation coefficient r) using Coloc 2 plugin (ImageJ). F4/80 showed significantly more colocalization than CD45 ($p =$ value 0.0074, nonpaired t test, 5–10 microscopical areas were analyzed).

enhanced binding and extravasation of liposomes in these areas. Further studies are therefore necessary to understand the molecular mechanisms of skin transport and the receptors involved in binding to skin endothelium.

CONCLUSIONS

This study has several important implications for drug delivery. Thus, it is evident that PEGylated liposomes accumulate more efficiently in the skin than non-PEGylated liposomes, partially due to their prolonged circulation times. At the same time, liposomal accumulation in the skin involves interaction with the endothelium, extravasation, and uptake by phagocytes in the dermis and subdermis, suggesting that PEGylated coating of liposomes cannot prevent these processes. Understanding the mechanism of these phenomena may lead to development of new strategies to prevent skin accumulation and improve the safety of chemotherapy-loaded liposomes and nanoparticles. Conversely, while liposomes have long been used for topical skin delivery for pharmaceuticals, vaccines, and cosmetics,^{48,49} the skin delivery via systemic injection has not been considered sufficiently. Understanding the mechanism of skin uptake can

open up possibilities to improve delivery of antigens and therapeutics to this tissue.

METHODS

Materials. Dextran 2000000 Da labeled with fluorescein isothiocyanate (FITC) was obtained from Sigma-Aldrich (St. Louis, MO). Egg phosphatidylcholine (EPC), hydrogenated soy phosphatidylcholine (HSPC), cholesterol, distearyl phosphatidylethanolamine (DSPE)-PEG-2000, DSPE-PEG-700, and DSPE-PEG-350 were obtained from Avanti Polar Lipids (Alabaster, AL), DiI (1,1'-dioctadecyl-3,3',3'-tetramethylindotricarbocyanine iodide) and DiI (1,1'-dioctadecyl-3,3',3'-tetramethylindocarbocyanine perchlorate) were obtained from Biotium (Hayward, CA). Whatman Nucleopore Track-Etch Membranes (0.2 and 0.1 μm pore size) were obtained from Sigma-Aldrich (St. Louis, MO). Nitrocellulose membrane was obtained from Bio-Rad. FITC-dextran (2MDa) was obtained from Sigma. Hoechst 33342 trihydrochloride trihydrate was obtained from Thermo Fischer, Waltham, MA). PEGylated liposomal doxorubicin (LipoDox, Sun Pharma) was obtained from the University of Colorado hospital pharmacy and stored at 4 $^{\circ}\text{C}$ prior to use. Antimouse F/80, antimouse CD41, and antimouse CD45 antibodies were all from BioLegend (San Diego, CA). Secondary antibodies (AlexaFluor 488 labeled) were from Thermo Fisher.

Preparation of Liposomes. PEGylated and non-PEGylated liposomes were prepared according to the compositions stated in Table 1. Whenever DSPE-PEG-350 or DSPE-PEG-750 were included at 5 mol %, the amount of EPC was decreased accordingly. The solutions of lipids in chloroform were mixed and dried under nitrogen stream. The dry lipid cake was resuspended in 1xPBS and subjected to three “freeze–thaw” cycles. The solution was brought to 10 mM total lipid by adding PBS and was extruded using an Avestin manual extruder (Avestin, Ottawa, Canada) through Whatman Nucleopore Track-Etch Membranes, through at least 30 extrusion cycles. EPC-based liposomes were extruded through a 0.2 mm membrane, whereas HSPC based liposomes were extruded through 0.2 μm and then 0.1 μm with heating. A Zetasizer Nano (Malvern, UK) was used to measure the size of the liposomes in 1xPBS. Liposomes were stored at 4 °C at a final concentration of 2 mM lipid for a maximum period of 2 months before use.

Mice. The University of Colorado Institutional Animal Care and Use Committee (IACUC) approved all animal experiments (protocol 103913(11)ID). Mice were treated according to regulations provided by the Office of Laboratory Animal Resources at the UC. Wild-type BALB/c mice were used for majority of experiments and bred in house. For testing C3 complement, C3 KO mice in C57/BL6 background and C57/BL6 wild type mice were obtained from Dr. VM Holers at the University of Colorado. Female mice at 6–10 weeks of age were used.

Near-Infrared Measurements of Fluorescence in the Skin, Blood, and Organs. The fiber optical near-infrared spectroscopy (FONIRS) has been described in detail elsewhere.¹² The system consists of a Maya 2000 Pro spectrometer with OceanView 1.5.0 software (both Ocean Optics) connected to a custom-built 600 μm excitation/emission probe via fiber-optic bundle (all from Ocean Optics, San Jose, CA). The FONIRS system uses LED with a peak emission wavelength of 760 nm as an excitation light source (Prizmatix Ltd., Givat-Shmuel, Israel). The in-line BrightLine filters (Semrock Inc., Rochester NY) were 785 nm short-pass (excitation) and 785 nm long-pass (emission). The emission was collected over a range of 800–840 nm. The integrated fluorescence (IF) was an integration of the spectral intensity over that wavelength range and used as the final measurement output.

For FONIRS experiments, mice were anesthetized with ketamine/xylazine (2 mg/0.32 mg per mouse), and the right flank was depilated using Nair hair removal cream. Skin was washed with warm water to prevent irritation from leftover cream. One day after depilation, DiR-labeled liposomes were injected via tail vein (200 $\mu\text{mol}/\text{mouse}$), and skin integrated fluorescence was measured with FONIRS in the depilated flank. Three measurements per time point were taken, and each measurement was the average of 2 scans with 800 ms integration time. Blood was collected via the retro-orbital sinus from each mouse at the same time points as FONIRS measurements postinjection.

In order to calculate the deposition in the skin at each time point using FONIRS measurements, first the integrated fluorescence values of noninjected skin (background) were subtracted from each time point. Since the signal in the skin is composed of the skin-deposited fluorescence and blood pool fluorescence, and assuming that 100% of skin signal at 30 s postinjection (first measurement time point) comes from the circulating liposomes, the deposition in the skin at subsequent time points was calculated as

$$IF_t^{\text{corrected}} = IF_t^{\text{total}} \times (1 - B_t)$$

where $IF_t^{\text{corrected}}$ is the blood pool-corrected integrated fluorescence at time t ; IF_t^{total} is the total integrated fluorescence at time t ; B_t is the fraction of liposomes remaining in blood at time t .

For organ distribution, injected and control mice were sacrificed and the organs were placed in wells of a 12-well plate. Skin around the torso of each mouse was also collected after the final time point. Organs were scanned with Li-COR Odyssey (intensity of 1.0 at both wavelengths (700 and 800 nm)). Mean fluorescence of the skin was determined from 16-bit images using ImageJ software by subtracting the background, drawing a ROI around the organs, and using a measure function to determine mean gray value.

Circulation Half-Life Measurements. In order to determine liposomal circulation half-life, 2 μL of plasma collected at different time points were applied in duplicates on a 0.22 μm nitrocellulose membrane and scanned at 800 nm using Li-COR Odyssey (for DiR liposomes) or at 565 nm using Bio-Rad gel camera (for DiI liposomes). The spot integrated density of a 16-bit TIFF image was measured with ImageJ and plotted as a function of time with Prism (GraphPad, San Diego CA). A nonlinear regression curve-fitting algorithm was used to fit the elimination profile into a mono-exponential decay to determine half-life.

Intravital Microscopy. BALB/c mice were preinjected with liposomes prior to the imaging experiment. An upright 3i VIVO spinning disk confocal microscope (Intelligent Imaging Innovations, Inc., Denver, CO) equipped with a Zeiss Plan Apochromat 20x/1.0 NA water immersion objective and 405, 488, 561 nm laser lines was used. Image acquisition and 3D reconstruction and editing was done using SlideBook 6 software (Intelligent Imaging Innovations, Inc.). Mice were continuously anesthetized with isoflurane via tubing connected to a Supera M1000 anesthesia evaporator machine (Supera, Clackamas, OR). The skin flap was formed in a previously described approach.^{50,51} Abdominal skin was incised, and a flap was formed by detaching the skin from the underlying tissue while preserving as many supplying blood vessels as possible. The skin flap (while still connected to the body) was immobilized by pinning it to a styrofoam plate and then washed with PBS to remove any spilled blood. Care was taken not to overstretch the flap. The rest of the mouse was also pinned to the plate, and several pins were attached between the trunk and the flap in order to prevent respiratory drift (as described in Figure 1D). The mouse was administered i.v. with 100 μL of 2 mg/mL of FITC-dextran and 4 mg/mL of Hoechst in PBS. The visceral (subdermal) part of the skin was placed under the objective. For continuous videomicroscopy (Figure 1F), a random area with intact blood flow (dextran-positive blood vessels) was quickly found and acquisition started in a time-lapse (movie) mode at 1 frame per 3 s, for duration of 2 h 15 min. For a single time point, intravital images (Figure 1E, 2C, 3C, and 5A) of each mouse were used once, and no long-term observations (longer than 10 min) were performed. For example, for 30 min imaging time point, mice were preinjected 30 min before the microscopy (approximately 15 min before skin flap preparation). The exception was the 5 min time point, where mice were injected with liposomes after the flap was formed. Areas with liposomal accumulation, and intact blood flow (dextran positive vessels) were quickly located, and images were taken in Z-series (depth) mode at 0.5–1 μm slice thickness (between 50 and 100 slices per image). At least five different areas of the flap (per time point) were taken. For image enhancement, the same settings were applied to all frames in Z-stacks and time-lapse sequences. In addition, selective time frames were individually enhanced in order to account for photobleaching and/or clearance of fluorescence over time.

Fluorescence Microscopy. For low magnification imaging of skin pieces, mice were euthanized 7 days postinjection, hairs on abdomen and belly were shaved, and skin pieces (approximately 4 × 3 cm) were excised and sandwiched between two microscopy slides. The slide sandwich was placed on a microscope stage (subdermal side toward the objective) and imaged at 25× magnification (EC Plan-NEO-FLUAR 2.5× objective) with Zeiss Axio Observer 5 epifluorescent microscope equipped with an X-Cite 200DC light source and AxioCam 506 monochromatic camera. For histological sections, mouse organs 7 days postinjection of liposomes were snap frozen in acetone/isopentane, cryosectioned into 10–15 μm sections, fixed with 4% (w/v) formalin, and stained for various cell surface markers as described in Figure 5. The Observer 5 microscope setup above was also used for near-infrared imaging of DiR labeled liposomes in histological sections (filter set for Cy7, catalog no. 49007, Chroma Corporation (McHenry, IL)).

Neutrophil Depletion. Mice were treated with monoclonal anti-Ly6C antibody (clone 1A8, BioLegend) as described previously.³¹ Briefly, mice were injected i.p. with 180 μg of the antibody 2 days prior to injection of EPC/DSPE-PEG₂₀₀₀/DiR/DiI liposomes. One day after liposomal injection, mice received an additional boost of the antibody

(100 μg i.p.). The mouse skin was imaged via intravital microscope 7 days postinjection, and the skin was isolated post-mortem and imaged with Li-COR at 800 nm.

ASSOCIATED CONTENT

Supporting Information

The Supporting Information is available free of charge on the ACS Publications website at DOI: 10.1021/acsnano.7b06524.

Figures S1–S4 (PDF)

Video: non-PEGylated liposomes, 4 h postinjection (ZIP)

Video: non-PEGylated liposomes, 24 h postinjection (ZIP)

Video: non-PEGylated liposomes, 2 h longitudinal monitoring postinjection (ZIP)

Video: PEGylated liposomes, 30 min postinjection (ZIP)

Video: PEGylated liposomes, 7 days postinjection (ZIP)

Video: LipoDox, 3 h postinjection (ZIP)

Video: LipoDox, 48 h postinjection (MOV)

AUTHOR INFORMATION

Corresponding Author

*E-mail: dmitri.simberg@ucdenver.edu.

ORCID

Seyed Moein Moghimi: 0000-0003-0836-926X

Dmitri Simberg: 0000-0002-5288-6275

Notes

The authors declare no competing financial interest.

ACKNOWLEDGMENTS

The funding supporting the study was from the National Institutes of Health CA194058 (to D.S.) and the Small Equipment Grant Program from the Skaggs School of Pharmacy and Pharmaceutical Sciences, University of Colorado (D.S.). Imaging experiments were performed in the University of Colorado Anschutz Medical Campus Advanced Light Microscopy Core supported in part by Rocky Mountain Neurological Disorders Core Grant No. P30NS048154 and by NIH/NCATS Colorado CTSI Grant No. UL1 TR001082.

REFERENCES

- (1) D'Mello, S. R.; Cruz, C. N.; Chen, M. L.; Kapoor, M.; Lee, S. L.; Tyner, K. M. The Evolving Landscape of Drug Products Containing Nanomaterials in the United States. *Nat. Nanotechnol.* **2017**, *12*, 523–529.
- (2) Lotem, M.; Hubert, A.; Lyass, O.; Goldenhersh, M. A.; Ingber, A.; Peretz, T.; Gabizon, A. Skin Toxic Effects of Polyethylene Glycol-Coated Liposomal Doxorubicin. *Arch. Dermatol.* **2000**, *136*, 1475–1480.
- (3) Gabizon, A.; Goren, D.; Horowitz, A. T.; Tzemach, D.; Lossos, A.; Siegal, T. Long-Circulating Liposomes for Drug Delivery in Cancer Therapy: A Review of Biodistribution Studies in Tumor-Bearing Animals. *Adv. Drug Delivery Rev.* **1997**, *24*, 337–344.
- (4) Yuan, Y.; Orlow, S. J.; Curtin, J.; Downey, A.; Muggia, F. Pegylated Liposomal Doxorubicin (PlD): Enhanced Skin Toxicity in Areas of Vitiligo. *Ecancermedicalscience* **2008**, *2*, 111.
- (5) Yuan, F.; Leunig, M.; Huang, S. K.; Berk, D. A.; Papahadjopoulos, D.; Jain, R. K. Microvascular Permeability and Interstitial Penetration of Sterically Stabilized (Stealth) Liposomes in a Human Tumor Xenograft. *Cancer Res.* **1994**, *54*, 3352–3356.
- (6) Huang, S. K.; Martin, F. J.; Jay, G.; Vogel, J.; Papahadjopoulos, D.; Friend, D. S. Extravasation and Transcytosis of Liposomes in Kaposi's Sarcoma-Like Dermal Lesions of Transgenic Mice Bearing the Hiv Tat Gene. *Am. J. Pathol.* **1993**, *143*, 10–14.

- (7) Gabizon, A.; Price, D. C.; Huberty, J.; Bresalier, R. S.; Papahadjopoulos, D. Effect of Liposome Composition and Other Factors on the Targeting of Liposomes to Experimental Tumors: Biodistribution and Imaging Studies. *Cancer Res.* **1990**, *50*, 6371–6378.

- (8) Hwang, K. J.; Padki, M. M.; Chow, D. D.; Essien, H. E.; Lai, J. Y.; Beaumier, P. L. Uptake of Small Liposomes by Non-Reticuloendothelial Tissues. *Biochim. Biophys. Acta, Biomembr.* **1987**, *901*, 88–96.

- (9) Charrois, G. J.; Allen, T. M. Multiple Injections of Pegylated Liposomal Doxorubicin: Pharmacokinetics and Therapeutic Activity. *J. Pharmacol. Exp. Ther.* **2003**, *306*, 1058–1067.

- (10) Sykes, E. A.; Dai, Q.; Tsoi, K. M.; Hwang, D. M.; Chan, W. C. W. Nanoparticle Exposure in Animals Can Be Visualized in the Skin and Analysed Via Skin Biopsy. *Nat. Commun.* **2014**, DOI: 10.1038/ncomms4796.

- (11) Cai, W.; Shin, D. W.; Chen, K.; Gheysens, O.; Cao, Q.; Wang, S. X.; Gambhir, S. S.; Chen, X. Peptide-Labeled near-Infrared Quantum Dots for Imaging Tumor Vasculature in Living Subjects. *Nano Lett.* **2006**, *6*, 669–676.

- (12) Griffin, J. I.; Benchimol, M. J.; Simberg, D. Longitudinal Monitoring of Skin Accumulation of Nanocarriers and Biologicals with Fiber Optic near Infrared Fluorescence Spectroscopy (Fonirs). *J. Controlled Release* **2017**, *247*, 167–174.

- (13) Petersen, S.; Fahr, A.; Bunjes, H. Flow Cytometry as a New Approach to Investigate Drug Transfer between Lipid Particles. *Mol. Pharmaceutics* **2010**, *7*, 350–363.

- (14) Shi, G.; Mukthavaram, R.; Kesari, S.; Simberg, D. Distearoyl Anchor-Painted Erythrocytes with Prolonged Ligand Retention and Circulation Properties *in vivo*. *Adv. Healthcare Mater.* **2014**, *3*, 142–148.

- (15) Gullapalli, R. R.; Demirel, M. C.; Butler, P. J. Molecular Dynamics Simulations of Dii-C18(3) in a Dppc Lipid Bilayer. *Phys. Chem. Chem. Phys.* **2008**, *10*, 3548–3560.

- (16) Allen, C.; Dos Santos, N.; Gallagher, R.; Chiu, G. N.; Shu, Y.; Li, W. M.; Johnstone, S. A.; Janoff, A. S.; Mayer, L. D.; Webb, M. S.; Bally, M. B. Controlling the Physical Behavior and Biological Performance of Liposome Formulations through Use of Surface Grafted Poly(Ethylene Glycol). *Biosci. Rep.* **2002**, *22*, 225–250.

- (17) Pittet, M. J.; Weissleder, R. Intravital Imaging. *Cell* **2011**, *147*, 983–991.

- (18) Chauhan, V. P.; Stylianopoulos, T.; Martin, J. D.; Popovic, Z.; Chen, O.; Kamoun, W. S.; Bawendi, M. G.; Fukumura, D.; Jain, R. K. Normalization of Tumour Blood Vessels Improves the Delivery of Nanomedicines in a Size-Dependent Manner. *Nat. Nanotechnol.* **2012**, *7*, 383–388.

- (19) Ahl, P. L.; Bhatia, S. K.; Meers, P.; Roberts, P.; Stevens, R.; Dause, R.; Perkins, W. R.; Janoff, A. S. Enhancement of the *in Vivo* Circulation Lifetime of L-Alpha-Distearoylphosphatidylcholine Liposomes: Importance of Liposomal Aggregation Versus Complement Opsonization. *Biochim. Biophys. Acta, Biomembr.* **1997**, *1329*, 370–382.

- (20) Clementi, F.; Paladè, G. E. Intestinal Capillaries. I. Permeability to Peroxidase and Ferritin. *J. Cell Biol.* **1969**, *41*, 33–58.

- (21) Granger, D. N.; Taylor, A. E. Permeability of Intestinal Capillaries to Endogenous Macromolecules. *Am. J. Physiol.* **1980**, *238*, H457–464.

- (22) Devoisselle, J. M.; Begu, S.; Tourne-Peteilh, C.; Desmettre, T.; Mordon, S. *In vivo* Behaviour of Long-Circulating Liposomes in Blood Vessels in Hamster Inflammation and Septic Shock Models-Use of Intravital Fluorescence Microscopy. *Luminescence* **2001**, *16*, 73–78.

- (23) Damen, J.; Regts, J.; Scherphof, G. Transfer and Exchange of Phospholipid between Small Unilamellar Liposomes and Rat Plasma High Density Lipoproteins. Dependence on Cholesterol Content and Phospholipid Composition. *Biochim. Biophys. Acta, Lipids Lipid Metab.* **1981**, *665*, 538–545.

- (24) Allen, T. M. A Study of Phospholipid Interactions between High-Density Lipoproteins and Small Unilamellar Vesicles. *Biochim. Biophys. Acta, Biomembr.* **1981**, *640*, 385–397.

- (25) Kirby, C.; Clarke, J.; Gregoriadis, G. Effect of the Cholesterol Content of Small Unilamellar Liposomes on Their Stability *in vivo* and *in vitro*. *Biochem. J.* **1980**, *186*, 591–598.
- (26) Dai, Q.; Walkey, C.; Chan, W. C. Polyethylene Glycol Backfilling Mitigates the Negative Impact of the Protein Corona on Nanoparticle Cell Targeting. *Angew. Chem., Int. Ed.* **2014**, *53*, 5093–5096.
- (27) Kullberg, M.; Martinson, H.; Mann, K.; Anchordoquy, T. J. Complement C3-Mediated Targeting of Liposomes to Granulocytic Myeloid Derived Suppressor Cells. *Nanomedicine* **2015**, *11*, 1355–1363.
- (28) Inturi, S.; Wang, G.; Chen, F.; Banda, N. K.; Holers, V. M.; Wu, L.; Moghimi, S. M.; Simberg, D. Modulatory Role of Surface Coating of Superparamagnetic Iron Oxide Nanoworms in Complement Opsonization and Leukocyte Uptake. *ACS Nano* **2015**, *9*, 10758–10768.
- (29) Becker, H. M.; Chen, M.; Hay, J. B.; Cybulsky, M. I. Tracking of Leukocyte Recruitment into Tissues of Mice by *in situ* Labeling of Blood Cells with the Fluorescent Dye Cfda Se. *J. Immunol. Methods* **2004**, *286*, 69–78.
- (30) Scieszka, J. F.; Maggiora, L. L.; Wright, S. D.; Cho, M. J. Role of Complement C3 and C5 in the Phagocytosis of Liposomes by Human Neutrophils. *Pharm. Res.* **1991**, *8*, 65–69.
- (31) Puerta-Arias, J. D.; Pino-Tamayo, P. A.; Arango, J. C.; Gonzalez, A. Depletion of Neutrophils Promotes the Resolution of Pulmonary Inflammation and Fibrosis in Mice Infected with *Paracoccidioides brasiliensis*. *PLoS One* **2016**, *11*, e0163985.
- (32) Hettinger, J.; Richards, D. M.; Hansson, J.; Barra, M. M.; Joschko, A. C.; Krijgsveld, J.; Feuerer, M. Origin of Monocytes and Macrophages in a Committed Progenitor. *Nat. Immunol.* **2013**, *14*, 821–830.
- (33) Thomas, M. L. The Leukocyte Common Antigen Family. *Annu. Rev. Immunol.* **1989**, *7*, 339–369.
- (34) Gordon, S.; Lawson, L.; Rabinowitz, S.; Crocker, P. R.; Morris, L.; Perry, V. H., Antigen Markers of Macrophage Differentiation in Murine Tissues. In *Macrophage Biology and Activation*; Russell, S. W., Gordon, S., Eds.; Springer: Berlin, 1992; pp 1–37.
- (35) Malissen, B.; Tamoutounour, S.; Henri, S. The Origins and Functions of Dendritic Cells and Macrophages in the Skin. *Nat. Rev. Immunol.* **2014**, *14*, 417–428.
- (36) Moghimi, S. M.; Hunter, A. C. Capture of Stealth Nanoparticles by the Body's Defences. *Crit. Rev. Ther. Drug Carrier Syst.* **2001**, *18*, 527–550.
- (37) Moghimi, S. M.; Hedeman, H.; Muir, I. S.; Illum, L.; Davis, S. S. An Investigation of the Filtration Capacity and the Fate of Large Filtered Sterically-Stabilized Microspheres in Rat Spleen. *Biochim. Biophys. Acta, Gen. Subj.* **1993**, *1157*, 233–240.
- (38) Matsumura, Y.; Maeda, H. A New Concept for Macromolecular Therapeutics in Cancer Chemotherapy: Mechanism of Tumor-tropic Accumulation of Proteins and the Antitumor Agent Smancs. *Cancer Res.* **1986**, *46*, 6387–6392.
- (39) Roberts, W. G.; Palade, G. E. Increased Microvascular Permeability and Endothelial Fenestration Induced by Vascular Endothelial Growth Factor. *J. Cell Sci.* **1995**, *108*, 2369–2379.
- (40) Egawa, G.; Nakamizo, S.; Natsuaki, Y.; Doi, H.; Miyachi, Y.; Kabashima, K. Intravital Analysis of Vascular Permeability in Mice Using Two-Photon Microscopy. *Sci. Rep.* **2013**, *3*, 1932.
- (41) Gabizon, A.; Dagan, A.; Goren, D.; Barenholz, Y.; Fuks, Z. Liposomes as *in vivo* Carriers of Adriamycin: Reduced Cardiac Uptake and Preserved Antitumor Activity in Mice. *Cancer Res.* **1982**, *42*, 4734–4739.
- (42) Karmali, P. P.; Simberg, D. Interactions of Nanoparticles with Plasma Proteins: Implication on Clearance and Toxicity of Drug Delivery Systems. *Expert Opin. Drug Delivery* **2011**, *8*, 343–357.
- (43) Moriwaki, H.; Kume, N.; Sawamura, T.; Aoyama, T.; Hoshikawa, H.; Ochi, H.; Nishi, E.; Masaki, T.; Kita, T. Ligand Specificity of Lox-1, a Novel Endothelial Receptor for Oxidized Low Density Lipoprotein. *Arterioscler., Thromb., Vasc. Biol.* **1998**, *18*, 1541–1547.
- (44) Matarazzo, S.; Quitadamo, M. C.; Mango, R.; Ciccone, S.; Novelli, G.; Biocca, S. Cholesterol-Lowering Drugs Inhibit Lectin-Like Oxidized Low-Density Lipoprotein-1 Receptor Function by Membrane Raft Disruption. *Mol. Pharmacol.* **2012**, *82*, 246–254.
- (45) von Eckardstein, A.; Rohrer, L. Transendothelial Lipoprotein Transport and Regulation of Endothelial Permeability and Integrity by Lipoproteins. *Curr. Opin. Lipidol.* **2009**, *20*, 197–205.
- (46) Oh, N.; Park, J. H. Endocytosis and Exocytosis of Nanoparticles in Mammalian Cells. *Int. J. Nanomed.* **2014**, *9*, 51–63.
- (47) Sato, Y. T.; Umezaki, K.; Sawada, S.; Mukai, S. A.; Sasaki, Y.; Harada, N.; Shiku, H.; Akiyoshi, K. Engineering Hybrid Exosomes by Membrane Fusion with Liposomes. *Sci. Rep.* **2016**, *6*, 21933.
- (48) Weiner, N.; Lieb, L.; Niemiec, S.; Ramachandran, C.; Hu, Z.; Egbaria, K. Liposomes: A Novel Topical Delivery System for Pharmaceutical and Cosmetic Applications. *J. Drug Target* **1994**, *2*, 405–410.
- (49) Hanson, M. C.; Crespo, M. P.; Abraham, W.; Moynihan, K. D.; Szeto, G. L.; Chen, S. H.; Melo, M. B.; Mueller, S.; Irvine, D. J. Nanoparticulate Sting Agonists Are Potent Lymph Node-Targeted Vaccine Adjuvants. *J. Clin. Invest.* **2015**, *125*, 2532–2546.
- (50) Yamauchi, K.; Yang, M.; Jiang, P.; Xu, M.; Yamamoto, N.; Tsuchiya, H.; Tomita, K.; Moossa, A. R.; Bouvet, M.; Hoffman, R. M. Development of Real-Time Subcellular Dynamic Multicolor Imaging of Cancer-Cell Trafficking in Live Mice with a Variable-Magnification Whole-Mouse Imaging System. *Cancer Res.* **2006**, *66*, 4208–4214.
- (51) Simberg, D.; Duza, T.; Park, J. H.; Essler, M.; Pilch, J.; Zhang, L.; Derfus, A. M.; Yang, M.; Hoffman, R. M.; Bhatia, S.; Sailor, M. J.; Ruoslahti, E. Biomimetic Amplification of Nanoparticle Homing to Tumors. *Proc. Natl. Acad. Sci. U. S. A.* **2007**, *104*, 932–936.